Journal of Computational and Applied Mathematics 340 (2018) 629–644

Contents lists available at ScienceDirect

Journal of Computational and Applied Mathematics

journal homepage: www.elsevier.com/locate/cam

Parametric domain decomposition for accurate reduced order models: Applications of MP-LROM methodology

Razvan Stefanescu [a], Azam Moosavi [b,*], Adrian Sandu [b]

[a] *Global Validation Model Department, Spire Global, Inc., Boulder, CO, United States*
[b] *Computational Science Laboratory, Department of Computer Science, Virginia Polytechnic Institute and State University, Blacksburg, VA 24060, United States*

ARTICLE INFO

Article history:
Received 1 June 2017
Received in revised form 3 November 2017

Keywords:
Local reduced-order models
Proper Orthogonal Decomposition
Regression machine learning techniques
Interpolation methods
Grassmann manifold

ABSTRACT

The multivariate predictions of local reduced-order-models (MP-LROM) methodology, recently proposed by the authors Moosavi et al. (0000), uses machine learning based regression methods to predict the errors of reduced-order models. This study considers two applications of MP-LROM. First, the error model is used in conjunction with a greedy sampling algorithm to generate decompositions of one dimensional parametric domains with overlapping regions, such that the associated local reduced-order models meet the prescribed accuracy requirements. Once a parametric domain decomposition is constructed, any parametric configuration belongs to (at least) one of the partitions; the local reduced-order model associated with that partition approximates the full order model at the given parameters within an accuracy level that is estimated a-priori. The parameter domain decomposition creates a database of the available local bases, local reduced-order, and high-fidelity models, and identifies the most accurate solutions for an arbitrary parametric configuration. Next, this database is used to enhance the accuracy of the reduced-order models using: (1) Lagrange interpolation of reduced bases in the matrix space; (2) Lagrange interpolation of reduced bases in the tangent space of the Grassmann manifold; (3) concatenation of reduced bases followed by a Gram–Schmidt orthogonalization process; and (4) Lagrange interpolation of high-fidelity model solutions. Numerical results with a viscous Burgers model illustrate the potential of the MP-LROM methodology to improve the design of parametric reduced-order models.

1. Introduction

Many physical phenomena in science and engineering are investigated today using large-scale computer simulation models. The ever-increasing complexity of these high-fidelity models poses considerable challenges related to computational time, memory requirements, and communication overhead in a parallel environment. A popular approach to alleviate these challenges is to construct inexpensive surrogate (approximate) models that capture the most important dynamical characteristics of the underlying physical models, but reduce the computational complexity by orders of magnitude. Examples of surrogates include response surfaces, low resolution models, and reduced-order models.

Reduced-order modeling uses snapshots of high-fidelity model solutions at different times to extract a low-dimensional subspace that captures most of the high-fidelity solution energy. The reduced-order surrogate is obtained by projecting the dynamics of the high-fidelity model onto the low-dimensional subspace. This is usually achieved by orthogonal or oblique

* Corresponding author.
E-mail address: azmosavi@vt.edu (A. Moosavi).

https://doi.org/10.1016/j.cam.2017.11.018
0377-0427/

projections coined as Galerkin or Petrov–Galerkin methods where the solution is searched as a linear combination of the basis vectors. Since the Galerkin method is actual an elliptic approach, applying it to hyperbolic models must be done with careful consideration [1]. The reduced dimension leads to a considerable reduction in computational complexity at the expense of a decreased solution accuracy. A reduced-order model approximates well the high-fidelity solution at a given point of operation (e.g., for the model parameter values for which the snapshots have been taken), but becomes less accurate away from that point (e.g., when the high-fidelity model is run with different parameter values).

To be useful, reduced-order models must accommodate changes over the entire parametric space without losing their accuracy, simplicity and robustness. Reduced-order model (ROM) accuracy and robustness can be achieved by constructing a global basis [2,3], but this strategy generates large dimensional bases that may lead to slow reduced-order models. Moreover, for fluid flows, the Galerkin expansion with global modes presumes synchronized flow dynamics. Whereas this assumption is true for internal flows, it is not suited for transient shear flows with uni-directional'hyperbolic' convection of vortices [4]. Changes in the operational settings may lead to deformation of leading flow structures [5] especially if the model is characterized by bifurcations and multiple attractors. Approaches such as limiting the operational setting, extending the mode sets [6] and offline/online set adaptation address the issue of mode deformation.

In localization approaches, the reduced-order models are built offline and one is chosen depending on the current state of the system. Local approaches have been designed for parametric [7,8] or state spaces generating local bases for both the state variables [9,10] and non-linear terms [8,11]. Dictionary approaches [12,13] pre-compute offline many basis vectors and then adaptively select a small subset during the online stage. Error bounds for reduced-order approximations of parametrized parabolic partial differential equations are available in [14].

In this study, we employ machine learning regression models to guide the construction of parametric space decompositions for solving parametric partial differential equations using accurate local reduced-order models. Whereas the current methodologies are defined in the sense of Voronoi tessellation and rely on K-means algorithms, our approach delimitates subregions of the parametric space by applying an Artificial Neural Networks model to estimate the errors of reduced-order models following a parametric domain sampling algorithm.

Machine learning methodologies have been applied to predict and model the approximation errors of low-fidelity and surrogate models [15–17]. The multi-fidelity correction (MFC) approach [18–21] has been developed to approximate the low-fidelity models errors in the context of optimization. The reduced order model error surrogates method (ROMES) [22] seeks to estimate full errors from indicators such as error bounds and reduced-order residual norms. Both ROMES and MFC models predict the error of global reduced-order models with fixed dimension using univariate functions.

In contrast, the authors' multivariate predictions of local reduced-order-model method (MP-LROM) [23] proposes a multivariate model to compute the error of local reduced-order surrogates. A MP-LROM model based on Artificial Neural Network and a sampling algorithm are applied here to construct decompositions of the parametric domain for solving parametric partial differential equations using local reduced-order models that are accurate within an admissible prescribed threshold. The proposed strategy relies on a greedy algorithm that samples the vicinity of each parameter value used to generate a local reduced-order model and finds an open ball such that for all the parameters in the ball the error of the local reduced-order model is less than the desired threshold. The essential ingredient is the MP-LROM error model which approximates the error of reduced-order model. Then a greedy technique is used to sample the parametric domain and generates a feasible region where a specific local reduced-order model provides accurate solutions within a prescribed tolerance. The union of these feasible regions forms a decomposition of the parametric domain. Different thresholds lead to different domain decompositions. The current methodology is designed for one dimensional parametric spaces and it is applied to the viscous 1D-Burgers model. A decomposition for the viscosity domain is generated for various error thresholds. Once the decomposition is constructed there is no need to run the high-fidelity model again, since for each parameter value μ there exists a parameter μ_p, and the associated reduced-order model (basis and reduced operators), whose solution error is accurately estimated a-priori. The dimension K_{POD} of the local basis is usually small since it depends only on one high-fidelity model trajectory.

The decomposition leads to a database of available bases, local reduced-order models and high fidelity trajectory. This database can be used to generate more accurate reduced-order models for an arbitrary parametric configuration. Three different approaches are compared here; i.e., bases interpolation, bases concatenation, and high-fidelity model solutions combination. For the first method, we perform a Lagrangian interpolation of the bases in the matrix space [24], or linearly interpolate their projections onto some local coordinate systems [24,25]. The second method follows the idea of the spanning ROM introduced in [26], where a projection basis is created by concatenating some of the available bases for an arbitrary parameter. The third method interpolates the associated high-fidelity solutions and then extracts the singular vectors to generate a new basis and local reduced-order model.

The remainder of the paper is organized as follows. Section 2 reviews the construction of reduced-order surrogates for parametric high-fidelity models (where the dynamics depends on a set of model parameters). Section 3 introduces the new methodology for constructing decompositions of the parametric domain using MP-LROM error predictions. Then the potential of combining the existing information for generating more accurate reduced-order model is discussed. Section 4 presents the applications of the proposed methodologies to a viscous 1D-Burgers system. Conclusions are drawn in Section 5.

2. Parametrized reduced-order modeling

Proper Orthogonal Decomposition has been successfully applied in numerous applications such as compressible flow [27] and computational fluid dynamics [28–30], to mention a few. It can be thought of as a Galerkin approximation in the state variable built from functions corresponding to the solution of the physical system at specified time instances. In this paper we consider discrete inner products (Euclidean dot product), though continuous products may be employed as well.

Generally, an unsteady problem can be written in semi-discrete form as an initial value problem; i.e., as a system of nonlinear ordinary differential equations

$$\frac{d\mathbf{x}(\mu,t)}{dt} = \mathbf{F}(\mathbf{x},t,\mu), \quad \mathbf{x}(\mu,0) = \mathbf{x}_0 \in \mathbb{R}^{N_{\text{state}}}, \quad \mu \in \mathcal{P}. \tag{1}$$

The input-parameter μ typically characterizes the physical properties of the flow. By $\mathcal{P}$ we denote the input-parameter space. For a given parameter configuration μ_p we select an ensemble of N_t time instances of the flow $\mathbf{x}(\mu_p,t_1),\ldots,\mathbf{x}(\mu_p,t_{N_t}) \in \mathbb{R}^{N_{\text{state}}}$, where N_{state} is the total number of discrete model variables, and $N_t \in \mathbb{N}^*$. The POD method chooses an orthonormal basis $U_{\mu_p} = [\mathbf{u}_1^{\mu_p} \ \cdots \ \mathbf{u}_{K_{POD}}^{\mu_p}] \in \mathbb{R}^{N_{\text{state}}\times K_{POD}}$, such that the mean square error between $\mathbf{x}(\mu_p,t_i)$ and the POD expansion $\mathbf{x}_{\mu_p}^{\text{POD}}(t_i) = U_{\mu_p}\tilde{\mathbf{x}}_{\mu_p}(\mu,t_i)$, $\tilde{\mathbf{x}}_{\mu_p}(\mu,t_i) = U_{\mu_p}^T\mathbf{x}(\mu_p,t_i) \in \mathbb{R}^{K_{POD}}$, is minimized on average. The POD space dimension $K_{POD} \ll N_{\text{state}}$ is appropriately chosen to capture the dynamics of the flow as described in [23, Algorithm 2, Section 2].

Next, a Galerkin projection of the full model state (1) onto the space $\mathcal{X}^{K_{POD}}$ spanned by the POD basis elements is used to obtain the reduced-order model

$$\frac{d\tilde{\mathbf{x}}_{\mu_p}(\mu,t)}{dt} = U_{\mu_p}^T\,\mathbf{F}\left(U_{\mu_p}\tilde{\mathbf{x}}_{\mu_p}(\mu,t),t,\mu\right), \quad \tilde{\mathbf{x}}_{\mu_p}(\mu,0) = U_{\mu_p}^T\,\mathbf{x}_0. \tag{2}$$

The notation $\tilde{\mathbf{x}}_{\mu_p}(\mu,t)$ expresses the solution dependence on the varying parameter μ and also on μ_p the configuration whose associated high-fidelity trajectory was employed to generate the POD basis. While being accurate for $\mu = \mu_p$, the reduced model (2) may lose accuracy when moving away from the initial setting. Several strategies have been proposed to derive a basis that spans the entire parameter space. These include the reduced basis method combined with the use of error estimates [31,32,3], global POD [33,34], Krylov-based sampling methods [35,36], and greedy techniques [37,38]. The fundamental assumption used by these approaches is that a smooth low-dimensional global manifold characterizes the model solutions over the entire parameter domain. However, in order to ensure high accuracy of the reduced solution across the parameter space, the dimension of the reduced basis has to be increased in practice, leading to higher on-line computational costs. To alleviate this drawback we propose to generate decompositions of the parametric domain with overlapping feasible regions where local reduced-order models are accurate to within an admissible prescribed threshold. The decompositions are generated using MP-LROM error models [23] briefly discussed in the next section along with the proposed approach for generating decompositions.

3. MP-LROM error model and its application to parametric domain decomposition

The MP-LROM models [23] are multivariate input–output maps $\phi : \mathbf{z} \mapsto y$ that predict different characteristics of local parametric reduced-order models, such as the error with respect to the high-fidelity model solution or basis dimension.

In this study we are using the MP-LROM model designed to predict the error of local reduced-order models (2) of different basis dimensions. The model has the following form

$$\phi^e_{MP-LROM} : \{\mu, \mu_p, K_{POD}\} \mapsto \log \varepsilon^{HF}_{\mu,\mu_p,K_{POD}}. \tag{3}$$

The input features include the parameter value μ, the parameter value μ_p associated with the full model run that generated the basis U_{μ_p} and the dimension of the reduced manifold K_{POD}.

The reduced order model error depends heavily on the parameter μ and basis U_{μ_p}. Since the dynamics of the non-linear models are not homogeneous all over the parameter space, we see a lot of variations in the error of reduced-order model. The reduced model usually loses accuracy when moving away from $\mu = \mu_p$. Hence it is very important to a-priori estimate the error of reduced-order model. The target of the mapping is the logarithm of error of the reduced-order model solution at μ using the basis U_{μ_p} and the corresponding reduced operators

$$\begin{aligned}&\log \varepsilon^{HF}_{\mu,\mu_p,K_{POD}} = \\ &\log\left(\|\mathbf{x}(\mu,t_1) - U_{\mu_p}\tilde{\mathbf{x}}_{\mu_p}(\mu,t_1) \quad \mathbf{x}(\mu,t_2) - U_{\mu_p}\tilde{\mathbf{x}}_{\mu_p}(\mu,t_2) \quad \cdots \quad \mathbf{x}(\mu,t_{N_t}) - U_{\mu_p}\tilde{\mathbf{x}}_{\mu_p}(\mu,t_{N_t})\|_F\right),\end{aligned} \tag{4}$$

where $\|\cdot\|_F$ denotes the Frobenius norm.

The MP-LROM model employs the logarithm of the error instead of the error since the variability of the error due to the dynamics of the model along the parameter space is large and using the logarithm of the error decreases the variance in prediction as shown in the numerical experiments of [23].

In this paper, we approximate the MP-LROM error model (3) using Artificial Neural Networks. Artificial Neural Networks (ANN) detect the pattern of data by discovering the input–output relationships. The neurons in ANN are organized in layers. At least three layers of neurons (an input layer, a hidden layer, and an output layer) are required for construction of a neural network. In supervised learning the network is provided with samples from which it discovers the relations of inputs and outputs. In the training process, the ANN adjusts the weights of network in order to reproduce the desired outputs. The output of the network is compared with the true data, and the error is back-propagated through the network. The back propagation algorithm [39] uses a gradient descent method to adjust the parameters of network such that the error between the desired output and the output signal of the network is minimized [40]. This process is repeated during several iterations, until the network output is close to the true data [41].

For our experiments, a neural network with six hidden layers and hyperbolic tangent sigmoid activation function in each layer is used. The data set has nearly 12 000 samples as follows: 10 and 100 equally distributed values of μ_p and μ over the entire parameter region; i.e., $\mu_p \in \{0.1, 0.2, \ldots, 1\}$ and $\mu \in \{0.01, \ldots, 1\}$, 12 reduced basis dimensions K_{POD} spanning the interval $\{4, 5, \ldots, 14, 15\}$ and the reduced-order model logarithm of errors $\log \varepsilon^{HF}_{\mu,\mu_p,K_{POD}}$. Since all 10 parameters μ_p belong to the set of all 100 parameters μ, only 100 high-fidelity runs are needed to construct the entire data set of 12 000 samples. A five-fold cross-validation approach is taken to train and test the ANN [23] and finally the trained error model is used for domain decomposition as well as better design of reduced order models which is fully discussed in the following.

3.1. Designing the decomposition of the parametric domain

Motivated by the need of fast and accurate simulations along the entire parametric space, we propose an alternative to the global parametric approach where only a single basis and a single reduced order model is constructed. Our alternative relies on a series of local reduced bases and reduced order models whose solutions meet prescribed admissible error thresholds beyond the parametric configurations employed for bases' construction. A parametric region, where a local reduced order model constructed using a single high-fidelity model trajectory is accurate to within a prescribed threshold, is called a feasible region. We delimitate such a region by employing the MP-LROM error model and sampling the neighborhood of the parametric configuration used to construct the local reduced order model. Our solution consists in designing a reunion of feasible regions completely covering the entire parametric space. This decomposition of the parametric domain was obtained as the solution of the following problem.

Problem 1 (*Accurate Local Parametric ROMs*)**.** For an arbitrary parameter configuration $\mu \in \mathcal{P}$ construct a reduced-order model (2) that provides an accurate and efficient approximation of the high-fidelity solution (1)

$$\|\mathbf{x}(\mu, t_1) - U_{\mu_p}\tilde{\mathbf{x}}_{\mu_p}(\mu, t_1) \quad \mathbf{x}(\mu, t_2) - U_{\mu_p}\tilde{\mathbf{x}}_{\mu_p}(\mu, t_2) \quad \cdots \quad \mathbf{x}(\mu, t_{N_t}) - U_{\mu_p}\tilde{\mathbf{x}}_{\mu_p}(\mu, t_{N_t})\|_F \leq \bar{\varepsilon}, \tag{5}$$

for some prescribed admissible error level $\bar{\varepsilon} > 0$. The snapshots used to generate the basis U_{μ_p} and reduced operators can be obtained with any parametric configuration $\mu_p \in \mathcal{P}$.

Our methodology proposes to select a finite countable subset $\mathcal{I} = \{\mu_{p_j},\ j = 1, \ldots, M\} \subset \mathcal{P}$ and for each μ_{p_j}, a reduced order basis $U_{\mu_{p_j}}$ along with the reduced operators are constructed for $j = 1, \ldots, M$. We denote by $\mathcal{U}$ the set of bases $U_{\mu_{p_j}}$, $j = 1, \ldots, M$. If for each parameter configuration μ_{p_j} there exists an open ball $\mathcal{B}(\mu_{p_j}, r_j) \in \mathcal{P}$ such that, for all parameters $\mu \in \mathcal{B}(\mu_{p_j}, r_j)$, the reduced order solution $\tilde{\mathbf{x}}_{\mu_p}(\mu, t)$ satisfies (5) for $\mu_p = \mu_{p_j}$ and the parametric domain $\mathcal{P}$ is a subset of the union of all these open balls, we obtain the sought decomposition of the parametric domain.

Next we derive a condition that guarantees the actual reduced-order model error

$$\varepsilon^{HF}_{\mu,\mu_{p_j},K_{POD}} = \|\mathbf{x}(\mu, t_1) - U_{\mu_{p_j}}\tilde{\mathbf{x}}_{\mu_{p_j}}(\mu, t_1) \quad \mathbf{x}(\mu, t_2) - U_{\mu_{p_j}}\tilde{\mathbf{x}}_{\mu_{p_j}}(\mu, t_2) \quad \cdots \quad \mathbf{x}(\mu, t_{N_t}) - U_{\mu_{p_j}}\tilde{\mathbf{x}}_{\mu_{p_j}}(\mu, t_{N_t})\|_F, \tag{6}$$

depending on parameter configuration μ, parameter configuration μ_{p_j} and basis dimension K_{POD}, satisfies the prescribed admissible threshold $\varepsilon^{HF}_{\mu,\mu_{p_j},K_{POD}} \leq \bar{\varepsilon}$, for any arbitrary parameter configuration μ inside of an open ball.

Theorem 3.1. *If* $\lim_{\mu\to\mu_{p_j}} \|\mathbf{x}(\mu, t_1) - U_{\mu_{p_j}}\tilde{\mathbf{x}}_{\mu_{p_j}}(\mu, t_1) \quad \mathbf{x}(\mu, t_2) - U_{\mu_{p_j}}\tilde{\mathbf{x}}_{\mu_{p_j}}(\mu, t_2) \quad \cdots \quad \mathbf{x}(\mu, t_{N_t}) - U_{\mu_{p_j}}\tilde{\mathbf{x}}_{\mu_{p_j}}(\mu, t_{N_t})\|_F = \bar{\varepsilon}^*$, *and* $\bar{\varepsilon}^* \leq \frac{\bar{\varepsilon}}{2}$, *then there exists* $r_j > 0$ *such that* $\varepsilon^{HF}_{\mu,\mu_{p_j},K_{POD}} \leq \bar{\varepsilon}$ *is satisfied for all parameters* μ *inside the ball* $\mathcal{B}(\mu_{p_j}, r_j)$.

Proof. From $\lim_{\mu\to\mu_{p_j}} \|\mathbf{x}(\mu, t_1) - U_{\mu_{p_j}}\tilde{\mathbf{x}}_{\mu_{p_j}}(\mu, t_1) \quad \mathbf{x}(\mu, t_2) - U_{\mu_{p_j}}\tilde{\mathbf{x}}_{\mu_{p_j}}(\mu, t_2) \quad \cdots \quad \mathbf{x}(\mu, t_{N_t}) - U_{\mu_{p_j}}\tilde{\mathbf{x}}_{\mu_{p_j}}(\mu, t_{N_t})\|_F = \bar{\varepsilon}^*$, using the limit definition, we have that for all $\varepsilon > 0$, there exists another real number $\delta > 0$ such that

$$|\|\mathbf{x}(\mu, t_1) - U_{\mu_{p_j}}\tilde{\mathbf{x}}_{\mu_{p_j}}(\mu, t_1) \quad \mathbf{x}(\mu, t_2) - U_{\mu_{p_j}}\tilde{\mathbf{x}}_{\mu_{p_j}}(\mu, t_2) \quad \cdots \quad \mathbf{x}(\mu, t_{N_t}) - U_{\mu_{p_j}}\tilde{\mathbf{x}}_{\mu_{p_j}}(\mu, t_{N_t})\|_F - \bar{\varepsilon}^*| < \varepsilon,$$

for all μ satisfying $d(\mu, \mu_{p_j}) < \delta$. By taking $\varepsilon = \bar{\varepsilon}^*$ and $\delta = r_j$ we obtain that

$$\varepsilon^{HF}_{\mu,\mu_{p_j},K_{POD}} < 2\bar{\varepsilon}^* \leq \bar{\varepsilon},\ \forall \mu \in \mathcal{B}(\mu_{p_j}, r_j),$$

which completes the proof. □

The theoretical result allows to compute the reduced-order model error at $\mu = \mu_{p_j}$ at certain parametric configurations in the proximity of μ_p. Moreover, one may be able to make statements about the degree of smoothness of the solution in the parametric space, therefore placing a lower limit on $\bar{\varepsilon}$. A particular case is when the reduced solution error is monotonically decreasing with smaller distances $d(\mu, \mu_{p_j})$. A small radius $r_j > 0$ then can be simply obtained by sampling and computing the residuals of the high-fidelity model using the projected reduced-order model solution.

One can also test for linear behavior of the high-fidelity solution $\mathbf{x}(\mu, t)$ in a small neighborhood of μ_{p_j}. Another possible screening test consists in checking the derivatives $\frac{\partial \mathbf{x}}{\partial \mu}(\mu, t)$ at equally distributed parameter values across the neighborhood of μ_{p_j}. If the derivatives are small, then the high-fidelity solutions do not vary much inside the open ball and they can be well approximated in the reduced manifold spanned by $U_{\mu_{p_j}}$.

The decomposition construction process ends as soon as the entire parameter domain $\mathcal{P}$ is covered with a union of overlapping balls $\mathcal{B}(\mu_{p_j}, r_j),\ j = 1, \ldots, M$, corresponding to different reduced order bases and local models

$$\mathcal{P} \subset \bigcup_{j=1}^{M} \mathcal{B}(\mu_{p_j}, r_j), \tag{7}$$

such that for each $j = 1, 2, \ldots, M$ and $\forall \mu \in \mathcal{B}(\mu_{p_j}, r_j) \cap \mathcal{P}$, the error of the reduced-order model solution (2) satisfies $\varepsilon^{HF}_{\mu, \mu_{p_j}, K_{POD}} \leq \bar{\varepsilon}$. The number of balls M is finite only if the space of all high-fidelity solution over the entire parametric domain can be approximated with a finite number of low-dimensional linear subspaces. This extends the concept of a single global low-dimensional manifold [33,34]. The cardinality of $\mathcal{I}$ depends on the high-fidelity solution variability along the parameter space. In theory, less variability should lead to smaller values of M. For our reduced-order models to satisfy the accuracy threshold for the entire parametric domain, we have to select thresholds $\bar{\varepsilon}$ not smaller than the Kolmogorov K_{POD}-width [42] of the so-called solution manifold$\{\mathbf{x}(\mu, t),\ \mu \in \mathcal{P},\ t \in \{t_i\}_{i=1}^{N_t}\}$.

This approach is inspired from the construction of unsteady local reduced-order models where the time domain is split in multiple regions [9,11]. In this way the reduced basis dimension is kept small allowing for fast on-line simulations. The cardinality of $\mathcal{I}$ is inversely proportional with the prescribed level of accuracy $\bar{\varepsilon}$. As the desired error threshold $\bar{\varepsilon}$ decreases, the decomposition changes since usually the radii r_j are expected to become smaller, and more balls are required to cover the parametric domain; i.e., M is increased.

The construction of the parametric domain decomposition (7) using the local parametric reduced-order models requires the following ingredients

1. The ability to probe the vicinity of $\mu_{p_j} \in \mathcal{P}$ and to efficiently estimate the level of error $\varepsilon^{HF}_{\mu, \mu_{p_j}, K_{POD}}$ (6).
2. The ability to find $r_j > 0$ such that $\varepsilon^{HF}_{\mu, \mu_{p_j}, K_{POD}} \leq \bar{\varepsilon}$, for all $\mu \in \mathcal{B}(\mu_{p_j}, r_j) \cap \mathcal{P}$.
3. The ability to identify the location of a new $\mu^*_{p_\ell}$ (for the construction of a new local reduced-order model) given the locations of the previous local parameters $\mu_{p_j}, j = 1, \ldots, \ell - 1$, so that

$$\begin{aligned} &\mathcal{B}(\mu^*_{p_\ell}, r_\ell) \not\subset \left(\bigcup_{i=1}^{\ell-1} \mathcal{B}(\mu_{p_i}, r_i)\right), \\ &\mathcal{B}(\mu^*_{p_\ell}, r_\ell) \bigcap \left(\bigcup_{i=1}^{\ell-1} \mathcal{B}(\mu_{p_i}, r_i)\right) \neq \emptyset. \end{aligned} \tag{8}$$

The second condition in (8) assures that the decomposition will have no coverage gap; i.e., Eq. (7) is satisfied.

In practice, an approximated MP-LROM error model is used to sample the vicinity of μ_{p_j} and predicts the error for each sample parameter value μ. Based on these error predictions, we construct the ball $\mathcal{B}(\mu_{p_j}, r_j)$, or perhaps a larger set called a μ_{p_j}—feasible region, where the local reduced-order model is accurate to within the prescribed threshold $\bar{\varepsilon}$ according to the MP-LROM model. Since the approximated MP-LROM model has errors in its predictions, the precision is guaranteed only if the sum of the true reduced-order model error and approximated MP-LROM model error is smaller than $\bar{\varepsilon}$. For a one dimensional parametric domain, a greedy algorithm to be described in Section 4.2 is applied to identify the location of a new parametric configuration $\mu^*_{p_\ell}$ (for the construction of a new basis) depending on the locations of the previous $\mu_{p_i},\ i = 1, \ldots, \ell - 1$. We seek to impose (8), so the entire parametric domain $\mathcal{P}$ satisfies (7) after the decomposition construction is finished. Again this is not necessarily guaranteed since we employ an approximated MP-LROM error model for this task.

3.2. Combining available information for accurate local ROMs at arbitrary parametric configurations

We next solve another practical problem: given a collection of local reduced bases and operators and high fidelity trajectories computed at various locations in the parameter space, construct a hierarchy of the available bases and models producing the most accurate local parametric reduced-order solutions for an arbitrary viscosity parameter μ^*. For the parametric domain situated at the intersection of different feasible regions introduced in Section 3.1, we may improve the

reduced solution accuracy by assigning a new reduced-order model based on the already existing local bases or high-fidelity simulations. Moreover, if a hierarchy of local reduced bases, local reduced-order, and high-fidelity models is available for a parametric configuration μ^*, we can employ the top ranked bases and models to generate a new reduced-order model whose accuracy may be increased. This can be achieved by interpolation or concatenation of the underlying reduced bases or interpolation of the available high-fidelity solutions.

The POD method produces an orthogonal basis that approximately spans the state solution space of the model for a specific parameter configuration. Moving away from the initial parametric configuration may require the construction of new bases and reduced operators since the initial reduced-order model may not be accurate anymore. However, if states depend continuously on parameters, the POD basis constructed for one parameter configuration may approximately span the solution space at different parametric settings in a local vicinity.

Several methods to combine the available information to generate more accurate reduced-order models for arbitrary parameter configurations μ^* have been proposed in the literature. One is the interpolation of the available reduced-order bases $U_{\mu_{p_j}}$, $j = 1, \ldots, M$. The parametric dependence of the bases has been modeled with various linear and nonlinear spatially-dependent interpolants.

Here we discuss different strategies that involve Lagrange interpolation of bases in the matrix space and in the tangent space of the Grassmann manifold. In addition we propose to concatenate the available reduced bases followed by an orthogonalization process, and to interpolate the solutions of the high fidelity model as means to derive the reduced-order basis for a parameter configuration μ^*.

3.2.1. Basis interpolation

Lagrange interpolation of bases. Assuming the reduced manifold $\mathbf{U} : \mathcal{P} \rightarrow \mathbb{R}^{N_{\text{state}} \times K_{POD}}$ poses a continuous and linear dependency with respect to the parametric space, and if M discrete bases $U_{\mu_{p_j}} = \mathbf{U}(\mu_{p_j})$ have been already constructed for various parametric configurations μ_{p_j}, $j = 1, 2, \ldots, M$, then a basis corresponding to the new configuration μ^* can be obtained using Lagrange's interpolation formula

$$U_{\mu^*} = \sum_{j=1}^{M} U_{\mu_{p_j}} L_j(\mu^*), \qquad L_j(\mu^*) = \prod_{i \neq j} \frac{\mu^* - \mu_{p_i}}{\mu_{p_j} - \mu_{p_i}}. \tag{9}$$

It is worth mentioning that the resulting interpolated basis vectors are not orthogonal. One drawback of this approach is the lack of linear variation in the angles between pairs of reduced subspaces [24] spanned by the reduced bases $U_{\mu_{p_j}}$. Differential geometry results can be employed to alleviate these deficiencies.

Grassmann manifold. In the study proposed by Amsallem and Farhat [25], basis (matrix) interpolation was performed in the tangent space of the Grassmann manifold G at a careful selected point S representing a subspace spanned by one of the available reduced bases. It has been shown that Grassmann manifold can be endowed with a differentiable structure [43,44]; i.e., at each point S of the manifold a tangent space exists. The mapping from the manifold to the tangent space is called the logarithmic mapping, while the backward projection is referred to as exponential mapping [45]. According to [25], a new subspace S_{μ^*}, and its subsequent basis U_{μ^*}, associated with a new parameter μ^*, can be obtained by interpolating the reduced subspaces projections into the tangent space of the Grassmann manifold and then projecting back using the exponential mapping. The reduced subspaces $\{S_{\mu_{p_i}}\}_{i=1}^{M}$ are spanned by the already computed reduced bases $U_{\mu_{p_i}}$, $i = 1, \ldots, M$. The steps required by this methodology [25] are described in the Algorithm 1. A graphical description of the method is provided in Fig. 1.

According to [25], the subspace angle interpolation [24,46] is identical to the interpolation in a tangent space to the Grassmann manifold of two reduced-order bases. Consequently the latter methodology can be viewed as a generalization of the former approach.

3.2.2. Basis concatenation

Basis concatenation idea was introduced in [26] and emerged from the notion of a global basis [33,34]. In the global strategy, the existing high-fidelity snapshots corresponding to various parameter configurations are collected in a single snapshot matrix and then a matrix factorization is performed to extract the most energetic singular vectors. This global basis is then used to build reduced-order models for parameter values not included in the initial snapshots set.

Assuming $\mathbf{X}_{\mu_{p_1}}, \mathbf{X}_{\mu_{p_2}}, \ldots, \mathbf{X}_{\mu_{p_M}} \in \mathbb{R}^{N_{\text{state}} \times N_t}$ are the snapshots corresponding to M high-fidelity model trajectories, the following error estimate holds [47, Proposition 2.16]:

$$\bar{\mathbf{X}} = [\mathbf{X}_{\mu_{p_1}} \cdots \mathbf{X}_{\mu_{p_M}}] = \bar{U} \Lambda \bar{V}^T \text{ (SVD factorization)}, \tag{10a}$$

$$\|\bar{\mathbf{X}} - \bar{U}^d \underset{\sim}{\boldsymbol{X}}\|_F^2 = \sum_{i=K_{POD}+1}^{N_t} \lambda_i^2 = \mathcal{O}(\lambda_{K_{POD}+1}^2), \quad \bar{U}_{ij}^d = \bar{U}_{ij},\ i = 1, 2, \ldots, N_{\text{state}},\ j = 1, 2, \ldots, K_{POD}, \tag{10b}$$

where λ_i is the ith singular value of $\bar{\mathbf{X}}$, and $\underset{\sim}{\boldsymbol{X}} = [\bar{U}^d]^T \bar{\mathbf{X}} \in \mathbb{R}^{K_{POD} \times (MN_t)}$. In practice, usually $N_t < N_{\text{state}}$, so the snapshot matrices are rank deficient. In this case and when the reduced-order bases $U_{\mu_{p_1}}, \ldots, U_{\mu_{p_M}}$, corresponding to the trajectories

Algorithm 1 Interpolation in a tangent space to a Grassmann manifold [25]

1: Select a point $S_{\mu_{p_M}}$ of the manifold to represent the origin point for the interpolation spanned by the basis $U_{\mu_{p_M}}$.

2: The tangent space $\mathcal{T}_{S_{\mu_{p_M}}}$ and the subspaces $\{S_{\mu_{p_i}}\}_{i=1}^{m}$ are considered, with $m \leq M-1$. Each point $S_{\mu_{p_i}}$ sufficiently close to $S_{\mu_{p_M}}$ is mapped to a point of $\mathcal{T}_{S_{\mu_{p_M}}}$, using the logarithm map $\log_{S_{\mu_{p_M}}}$ [45]. The bases spanning the tangent space points $\log_{S_{\mu_{p_M}}}(S_{\mu_{p_i}})$ are computed by

$$(I - U_{\mu_{p_M}} U_{\mu_{p_M}}^T) U_{\mu_{p_i}} (U_{\mu_{p_M}} U_{\mu_{p_i}})^{-1} = R_i \Lambda_i Q_i^T \text{ (SVD factorization)},$$
$$\Gamma_{\mu_{p_i}} = R_i \tan^{-1}(\Lambda_i) Q_i^T.$$

3: Each entry of the matrix Γ_{μ^*} associated with the target parameter μ^* is computed by interpolating the corresponding entries of the matrices $\Gamma_{\mu_{p_i}} \in \mathbb{R}^{N_{state} \times K_{POD}}$ associated with the parameter points μ_{p_i}, $i = 1, \ldots, m$. A univariate or multivariate Lagrange interpolation may be chosen similar with the one introduced in (9).

4: The matrix Γ_{μ^*} representing a point in the tangent space $\mathcal{T}_{S_{\mu_{p_M}}}$ is mapped to a subspace S_{μ^*} on the Grassmann manifold spanned by a matrix U_{μ^*} using the exponential map [45]

$$\Gamma_{\mu^*} = R^* \Lambda^* Q^{*T} \text{ (SVD factorization)},$$
$$U_{\mu^*} = U_{\mu_{p_M}} Q^* \cos(\Lambda^*) + R^* \sin(\Lambda^*).$$

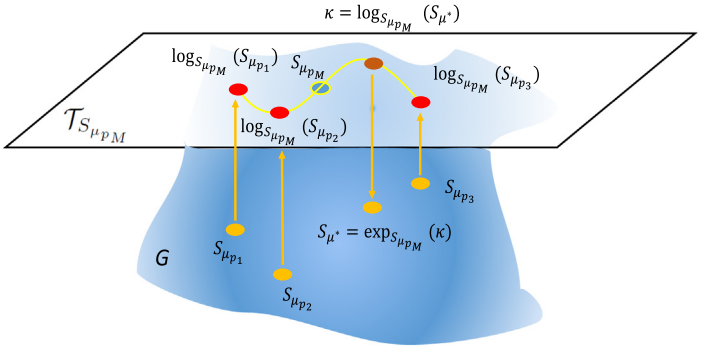

Fig. 1. The description of the interpolation of four subspaces in a tangent space to a Grassmann manifold. The origin point of the interpolation is $S_{\mu_{p_M}}$ and $m = 3$.

$\mu_{p_1}, \ldots, \mu_{p_M}$, are available, we can construct a basis $\hat{U}$ by simply concatenating columns of $U_{\mu_{p_1}}, \ldots, U_{\mu_{p_M}}$ such that the accuracy level in (10) is preserved.

Proposition 3.2. *Consider the following SVD of snapshots matrices* $\mathbf{X}_{\mu_{p_1}}, \ldots, \mathbf{X}_{\mu_{p_M}} \in \mathbb{R}^{N_{\text{state}} \times N_t}$

$$\mathbf{X}_{\mu_{p_j}} = U_{\mu_{p_j}} \Lambda_j V_{\mu_{p_j}}^T, \quad j = 1, 2, \ldots, M, \tag{11}$$

with $N_t < N_{\text{state}}$ *and* $rank(\mathbf{X}_{\mu_{p_i}}) < N_t$, $i = 1, 2, \ldots, M$. *Then, there exist positive integers* $K_{POD}^1, \ldots, K_{POD}^M$, *and* $\hat{\mathbf{X}} \in \mathbb{R}^{(\sum_{i=1}^{M} K_{POD}^i) \times (MN_t)}$, *such that* $\bar{\mathbf{X}}$ *defined in* (10) *satisfies*

$$\|\bar{\mathbf{X}} - \hat{U}\,\hat{\mathbf{X}}\|_F^2 \leq \mathcal{O}(\lambda_{K_{POD}+1}^2), \tag{12}$$

where $\lambda_{K_{POD}+1}$ *is the* $(K_{POD}+1)$ *singular value of snapshots matrix* $\bar{\mathbf{X}}$, *and* $\hat{U} = [U_{\mu_{p_1}}^d \ \cdots \ U_{\mu_{p_M}}^d] \in \mathbb{R}^{N_{\text{state}} \times (\sum_{i=1}^{M} K_{POD}^i)}$, $[U_{\mu_{p_l}}^d]_{ij} = [U_{\mu_{p_l}}]_{ij}$, $i = 1, 2, \ldots, N_{\text{state}}$, $j = 1, 2, \ldots, K_{POD}^i$, $l = 1, 2, \ldots, M$.

Proof. Since $\mathbf{X}_{\mu_{p_1}}, \ldots, \mathbf{X}_{\mu_{p_M}} \in \mathbb{R}^{N_{\text{state}} \times N_t}$ are rank deficient matrices, there exist at least M positive integers $K_{POD}^1, \ldots, K_{POD}^M$, such that the singular values associated with $\mathbf{X}_{\mu_{p_1}}, \ldots, \mathbf{X}_{\mu_{p_M}}$ satisfy

$$[\lambda_{K_{POD}^1+1}^1]^2, \ldots, [\lambda_{K_{POD}^M+1}^M]^2 \leq [\lambda_{K_{POD}+1}]^2, \ \forall K_{POD} = 0, \ldots, N_{t-1}. \tag{13}$$

From [47, Proposition 2.16] and (11) we have the following estimates

$$\|\mathbf{X}_{\mu_{p_j}} - U^d_{\mu_{p_j}} \underset{\sim}{\mathbf{X}}_{\mu_{p_j}}\|_F^2 = \sum_{i=K^j_{POD}+1}^{N_t} [\lambda^j_i]^2 = \mathcal{O}([\lambda^j_{K^j_{POD}+1}]^2) \leq \mathcal{O}([\lambda_{K_{POD}+1}]^2), \tag{14}$$

where λ^j_i is the ith singular value of $\mathbf{X}_{\mu_{p_j}}$ and $\underset{\sim}{\mathbf{X}}_{\mu_{p_j}} = [U^d_{\mu_{p_j}}]^T \mathbf{X}_{\mu_{p_j}} \in \mathbb{R}^{K^j_{POD} \times N_t}$, for $j = 1, \ldots, M$.

By denoting

$$\hat{\mathbf{X}} = \begin{bmatrix} \underset{\sim}{\mathbf{X}}_{\mu_{p_1}} & \mathbf{0}_1 & \cdots & \cdots & \mathbf{0}_1 \\ \mathbf{0}_2 & \underset{\sim}{\mathbf{X}}_{\mu_{p_2}} & \mathbf{0}_2 & \cdots & \mathbf{0}_2 \\ \vdots & \vdots & \vdots & \vdots & \vdots \\ \mathbf{0}_M & \cdots & \cdots & \mathbf{0}_M & \underset{\sim}{\mathbf{X}}_{\mu_{p_M}} \end{bmatrix},$$

where the null matrix $\mathbf{0}_j$ belongs to $\mathbb{R}^{K^j_{POD} \times N_t}$, $j = 1, \ldots, M$, we have

$$\|\bar{\mathbf{X}} - \hat{U}\,\hat{\mathbf{X}}\|_F^2 = \|[\mathbf{X}_{\mu_{p_1}} \ \cdots \ \mathbf{X}_{\mu_{p_M}}] - [U^d_{\mu_{p_1}} \underset{\sim}{\mathbf{X}}_{\mu_{p_1}} \ \cdots \ U^d_{\mu_{p_M}} \underset{\sim}{\mathbf{X}}_{\mu_{p_M}}]\|_F^2 \leq$$

$$\left(\sum_{i=1}^{M} \|\mathbf{X}_{\mu_{p_i}} - U^d_{\mu_{p_i}} \underset{\sim}{\mathbf{X}}_{\mu_{p_i}}\|_F\right)^2 = \sum_{i=1}^{M}\sum_{j=1}^{M} \|\mathbf{X}_{\mu_{p_i}} - U^d_{\mu_{p_i}} \underset{\sim}{\mathbf{X}}_{\mu_{p_i}}\|_F \cdot$$

$$\|\mathbf{X}_{\mu_{p_j}} - U^d_{\mu_{p_j}} \underset{\sim}{\mathbf{X}}_{\mu_{p_i}}\|_F \leq \mathcal{O}([\lambda_{K_{POD}+1}]^2). \quad \square$$

By assuming that $\text{rank}(\mathbf{X}_{\mu_{p_i}}) < N_t$, for all $j = 1, \ldots, M$, imposes N_t as an upper limit for all the positive integers K^i_{POD}, $j = 1, \ldots, M$. This assumption is not unrealistic since typically the snapshots matrix stores correlated data and therefore contains linearly dependent columns. For linearly independent matrices, the precision is controlled by the spectra of snapshots matrices $\mathbf{X}_{\mu_{p_i}}$, $i = 1, \ldots, M$, but there is no guarantee that the expansion based on the concatenated basis $\hat{U}$ can provide similar accuracy precision as the expansion based on $\bar{U}$ (10) for all $K_{POD} = 1, 2, \ldots, N_t$.

In practice usually $\sum_{i=1}^{M} K^i_{POD}$ is larger than K_{POD}, thus more bases functions are required to form $\hat{U}$ to achieve a similar level of precision as in (10) where $\bar{U}$ is built using a global singular value decomposition. According to [48], the faster approach to compute the left singular vectors and singular values only is to apply a QR factorization followed by a R-bidiagonalization [49]. The R-SVD decomposition of a matrix of dimension $N_{\text{state}} \times N_t$ has a computational complexity of $\mathcal{O}(4N^2_{\text{state}}N_t + 13N^3_t)$. As such, the decomposition of matrix $\bar{\mathbf{X}}$ requires $\mathcal{O}(4MN^2_{\text{state}}N_t + 13M^3N^3_t)$ operations, whereas all combined singular value decompositions of matrices $\mathbf{X}_{\mu_{p_i}}$, $i = 1, \ldots, M$, have a computational complexity of $\mathcal{O}(4MN^2_{\text{state}}N_t + 13MN^3_t)$. This estimation suggests that the matrix factorization of $\bar{\mathbf{X}}$ is more computationally demanding. However, the first term $4MN^2_{\text{state}}N_t$ often dominates as $N_t \ll N_{\text{state}}$ in practice, leading to almost similar computational times. The off-line stage of the concatenation method may also include the application of a Gram–Schmidt-type algorithm to orthogonalize the overall set of vectors in $\hat{U}$.

While the Lagrange interpolation of bases mixes the different energetic singular vectors in an order dictated by the singular values magnitude, this strategy concatenates the dominant singular vectors for each case and preserves their structure.

3.2.3. Interpolation of high-fidelity model solutions

The method discussed herein assumes that the model solution depends continuously on the parameters. Thus it is natural to consider constructing the basis for a parameter configuration μ^* by interpolating the existing high-fidelity model solutions associated with various parameter settings, and then performing the SVD of the interpolated results. For example, the Lagrange solution interpolant is given by

$$\mathbf{X}_{\mu^*} = \sum_{j=1}^{M} \mathbf{X}_{\mu_{p_j}} L_j(\mu^*), \tag{15}$$

where $\mathbf{X}_{\mu_{p_j}} \in \mathbb{R}^{N_{\text{state}} \times N_t}$ is the model solution corresponding to parameter μ_{p_j} and the interpolation polynomials are defined in (9).

A new basis is constructed from the interpolated model solution (15) for the new parametric configuration μ^*. From computational point of view the complexity of the off-line stage of the solution interpolation method (15) is smaller than in the case of the bases concatenation and interpolation approaches. Only one singular value decomposition is required in contrast with the multiple factorizations needed in the latter two strategies where the involved matrices have the same size $N_{\text{state}} \times N_t$. Having only N_t snapshots the size of the outcome basis should be smaller than in the case of basis concatenation approach.

4. Numerical experiments

We illustrate the application of the MP-LROM error model to design decompositions of the parametric domain for a one-dimensional Burgers model. Moreover, the database of accurate local bases, local reduced-order and high-fidelity models are used to enhance the accuracy of the reduced-order model for a different parametric configuration μ^*. For each of the applications introduced in Section 3, we present in detail the proposed solution approaches and the corresponding numerical results. The 1D-Burgers model proposed herein is characterized by one scalar viscosity parameter.

4.1. One-dimensional Burgers' equation

Burgers' equation is an important partial differential equation from fluid mechanics [50]. The evolution of the velocity u of a fluid evolves according to

$$\frac{\partial u}{\partial t} + u\frac{\partial u}{\partial x} = \mu\frac{\partial^2 u}{\partial x^2}, \quad x \in [0, L], \quad t \in (0, t_f], \tag{16}$$

with $t_f = 1$ and $L = 1$. Here μ is the viscosity coefficient.

The model has homogeneous Dirichlet boundary conditions $u(0, t) = u(L, t) = 0, t \in (0, t_f]$. For the initial conditions, we used a seventh order polynomial constructed using the least-square method and the data set {(0, 0); (0.2, 1); (0.4, 0.5); (0.6, 1); (0.8, 0.2); (0.9, 0.1); (0.95, 0.05); (1, 0)}.

The discretization uses a spatial mesh of N_s equidistant points on $[0, L]$, with $\Delta x = L/(N_s - 1)$. A uniform temporal mesh with N_t points covers the interval $[0, t_f]$, with $\Delta t = t_f/(N_t - 1)$. The discrete velocity vector is $\boldsymbol{u}(t_j) \approx [u(x_i, t_j)]_{i=1,2,\ldots,N_{\text{state}}} \in \mathbb{R}^{N_{\text{state}}}, j = 1, 2, \ldots, N_t$, where $N_{\text{state}} = N_s - 2$ (the known boundaries are removed). The semi-discrete version of the model (16) is

$$\mathbf{u}' = -\nu\mathbf{u} \odot A_x\boldsymbol{u} + \mu A_{xx}\boldsymbol{u}, \tag{17}$$

where $\mathbf{u}'$ is the time derivative of $\mathbf{u}$, and $A_x, A_{xx} \in \mathbb{R}^{N_{\text{state}} \times N_{\text{state}}}$ are the central difference first-order and second-order space derivative operators, respectively, which take into account the boundary conditions, too. The model is implemented in Matlab and the backward Euler method is employed for time discretization. The nonlinear algebraic systems are solved using the Newton–Raphson method and the allowed number of Newton iterations per each time step is set to 50. The solution is considered to have converged when the Euclidean norm of the residual is less then 10^{-10}.

The viscosity parameter space $\mathcal{P}$ is set to the interval [0.01, 1]. Smaller values of μ correspond to sharper gradients in the solution, and lead to dynamics more difficult to accurately approximate using reduced-order models.

The reduced-order models are constructed using POD method whereas the quadratic nonlinearities are computed via tensorial POD [51] for efficiency. The online and offline associated CPU times are provided in Fig. 2 of MP-LROM paper [23].

4.2. Designing the decomposition of the parametric domain

In the sequel, we present some of the details associated with the construction of ANN model approximating the MP-LROM error model (3). A full description is available in [23]. The whole data set contains 12 000 samples including 10 and 100 equally distributed values of μ_p and μ over the entire parameter region; i.e., $\mu_p \in \{0.1, 0.2, \ldots, 1\}$ and $\mu \in \{0.01, \ldots, 1\}$, 12 reduced basis dimensions K_{POD} spanning the interval $\{4, 5, \ldots, 14, 15\}$ and the reduced-order model logarithm of errors $\log \varepsilon^{HF}_{\mu,\mu_p,K_{POD}}$. The trained models were assessed by the common five-fold cross-validation technique using the Burger's model. The reported accuracy was 0.004004 [23, table 3].

The whole data set contains 12 000 samples. It is worth to note that, only one high-fidelity model simulation is required for computing the reduced solutions errors for the parametric configuration μ using reduced-order models of various K_{POD} and various bases and reduced operators constructed at μ_p. As such, only 100 high-fidelity simulations were needed to construct the entire data set due also to the fact that the set of parameters μ_p is a subset of the selected parameters μ. High-fidelity simulations are used to accurately calculate the errors associated with the existing reduced-order models for parametric configurations μ.

Next we seek to build a decomposition of the viscosity domain [0.01, 1] for the 1D-Burgers model using the ANN MP-LROM error model.

As discussed in Section 3, we take the following steps. First we identify "μ_p-feasible" intervals $[d_\ell, d_r]$ in the parameter space such that local reduced-order model depending only on the high-fidelity trajectory at μ_p is accurate to within the prescribed threshold for any $\mu \in [d_\ell, d_r]$. Second, a greedy algorithm generates the decomposition

$$[0.01, 1] \subset \bigcup_{i=1}^{M} \left[d_\ell^i, d_r^i\right], \tag{18}$$

by covering the parameter space with a union of μ_{p_i} feasible intervals, where each μ_{p_i}-feasible interval is characterized by an error threshold $\bar{\varepsilon}_i$ (which can vary from one interval to another). This relaxation is suggested since for intervals associated

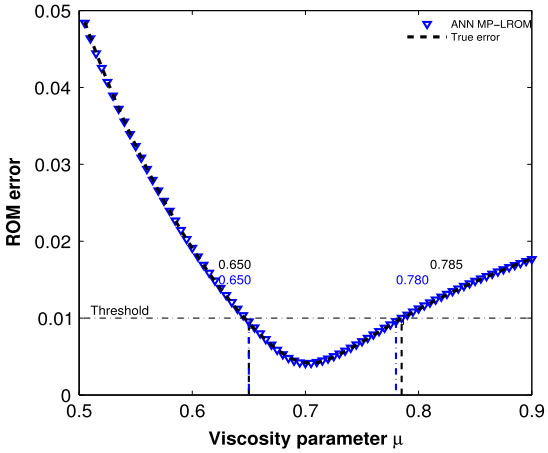

Fig. 2. The average range of parameter μ obtained with MP-LROM models for $K_{POD} = 9$ and $\mu_p = 0.7$. The desired accuracy is $\bar{\varepsilon} = 10^{-2}$. The numbers represent the left and the right edges of the predicted vs the true feasible intervals.

with small parameters μ_{p_i}, it is difficult to achieve small reduced-order models errors similar to those obtained for larger parametric configurations.

For the existing reduced basis methods a global reduced-order model depending on multiple high-fidelity trajectories is usually constructed. In contrast, our approach uses the ANN MP-LROM error model to decompose the parameter space into smaller regions where the local reduced-order model solutions are accurate to within some tolerance levels. Since the local bases required for the construction of the local reduced-order models depend on only a single full simulation, the dimension of the POD subspace is small, leading to lower on-line computational complexity.

Construction of a μ_p-feasible interval

The ANN MP-LROM error model can accurately estimate $\log \varepsilon^{HF}_{\mu,\mu_p,K_{POD}}$ (4) associated with reduced-order models. Thus we can employ it to establish a range of viscosity parameters around μ_p such that the reduced-order solutions depending on U_{μ_p} satisfy some desired accuracy level. More precisely, starting from parameter μ_p, a fixed POD basis dimension and a tolerance error $\log \bar{\varepsilon}$, we are searching for an interval $[d_l, d_r]$ such that the estimated prediction $\widehat{\log \varepsilon}^{HF}_{\mu,\mu_p,K_{POD}}$ of the true error $\log \varepsilon^{HF}_{\mu,\mu_p,K_{POD}}$ (4) meets the requirement

$$\widehat{\log \varepsilon}^{HF}_{\mu,\mu_p,K_{POD}} < \log \bar{\varepsilon}, \forall \mu \in [d_l, d_r]. \tag{19}$$

Our proposed strategy makes use of a simply incremental approach by sampling the vicinity of μ_p to account for the estimated errors $\widehat{\log \varepsilon}^{HF}_{\mu,\mu_p,K_{POD}}$ forecasted by the ANN MP-LROM error model. A grid of new parameters μ is built around μ_p and the error models predict the errors outward of μ_p. Once the error models outputs are larger than the prescribed error $\log \bar{\varepsilon}$, the previous μ satisfying the constraint (19) is set as d_l, for $\mu < \mu_p$ or d_r for $\mu > \mu_p$.

Fig. 2 illustrates the range of parameters predicted by the ANN MP-LROM model against the true feasible interval and the results show good agreement. For this experiment we set $\mu_p = 0.7$, dimension of POD subspace $K_{POD} = 9$ and $\bar{\varepsilon} = 10^{-2}$. Values of $\mu = \mu_p \pm 0.001 \cdot i$, $i = 1, 2, \ldots$ are passed to the ANN MP-LROM model. The average range of parameters obtained over five different configurations with ANN is [0.650, 0.780]. We trained the models with 80% random split of the data set and test it over the fixed test set of Fig. 2. For this design, the true range of parameters is [0.650, 0.785] underlying the predicting potential of MP-LROM model built using ANN technique.

The decomposition of the parametric domain as a union of μ_p-feasible intervals

A union of different μ_{p_k}-feasible intervals can be designed to cover a general entire 1D-parametric domain $[A, B]$. Once such construction is available, it will allow for reduced-order simulations with a-priori error quantification for any value of viscosity parameter $\mu \in [A, B]$.

A greedy strategy based on the ANN MP-LROM error model is described in Algorithm 2 and its output is a collection of feasible intervals $\cup_{k=1}^{n} [d_l^k, d_r^k] \supset [A, B]$. After each iteration k of the algorithm, a μ_{p_k}-feasible interval $[d_l^k, d_r^k]$ is constructed. Each interval is associated with some accuracy threshold $\bar{\varepsilon}_k$. For small viscous parametric values we found out that designing μ_{p_k}-feasible intervals associated with higher precision levels (very small thresholds $\bar{\varepsilon}_k$) is impossible since the dynamics of parametric 1D-Burgers model solutions change dramatically with smaller viscosity parameters. In consequence we decided to let $\bar{\varepsilon}_k$ vary along the parametric domain to accommodate the solution physical behavior. Thus a small threshold $\bar{\varepsilon}_0$ will

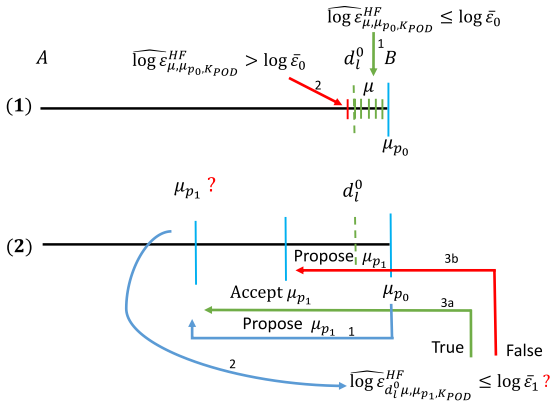

(a) Designing the first feasible interval (1) and selecting a new centered parameter μ_{p_1} (2)

(b) Designing a feasible interval (3) and increasing the tolerance level (4).

Fig. 3. A description of the most important stages of the parameter domain decomposition algorithm. The arrows describe the internal steps for each stage initiated in the order depicted by the arrows' indices. (For interpretation of the references to color in this figure legend, the reader is referred to the web version of this article.)

be initially set and as we will advance charting the parameter domain $[A, B]$ from right to left, the threshold $\bar{\varepsilon}_k$ will be increased.

The algorithm starts by selecting the first centered parameter μ_{p_0} responsible for basis generation. It can be set to $\mu_{p_0} = B$ but may take any value in the proximity of B, $\mu_{p_0} \leq B$. This choice depends on the variability of parametric solutions in this domain region and by selecting μ_{p_0} to differ from the right edge of the domain, the number n of the feasible intervals should decrease.

The next step is to set the threshold $\bar{\varepsilon}_0$ along with the maximum permitted size of the initial feasible interval to be constructed. This is set to $2 \cdot r_0$, thus r_0 can be referred as the interval radius. Along with the radius, the parameter Δr will decide the maximum number of ANN MP-LROM model calls employed for the construction of the first μ_{p_0}-feasible interval. While the radius is allowed to vary during the algorithm iterations, Δr is kept constant. Finally the dimension of POD basis has to be selected together with three parameters β_1, β_2 and β_3 responsible for changes in the threshold and radius and selecting a new parameter location μ_{p_k} encountered during the procedure.

Next the algorithm starts the construction of the μ_{p_0} feasible interval. The process is described in the top part of Fig. 3(a). Then we are sampling the vicinity of μ_{p_0} for equally distributed parameters μ and compute the ANN MP-LROM model predictions. The sampling process and the comparison between the predicted errors $\widehat{\log \varepsilon}^{HF}_{\mu,\mu_{p_0},K_{POD}}$ and $\log \bar{\varepsilon}_0$ are depicted in Fig. 3(a). A green vertical segment indicates that the estimated error satisfies the threshold; i.e., $\widehat{\log \varepsilon}^{HF}_{\mu,\mu_{p_0},K_{POD}} < \log \bar{\varepsilon}_0$, whereas the red segment indicates the opposite. The left limit of the μ_{p_0}-feasible interval is obtained when either $\mu > \mu_{p_0} - r_0$ or $\widehat{\log \varepsilon}^{HF}_{\mu,\mu_{p_0},K_{POD}} > \log \bar{\varepsilon}_0$. The left limit d_l^0, denoted with a green dashed line in Fig. 3(a), is set equal to the last parameter μ such that $\widehat{\log \varepsilon}^{HF}_{\mu,\mu_{p_0},K_{POD}} \leq \log \bar{\varepsilon}_0$.

The next step searches for a centered parameter $\mu_{p_{k+1}}$ and this process is described at the bottom of Fig. 3(a) for $k = 0$. The centered parameter $\mu_{p_{k+1}}$ is first proposed based on an empirical formula described in line 25 of Algorithm 2. This formula depends on the current centered parameter μ_{p_k}, the number of tested parameters μ during the construction of μ_{p_k}-feasible interval, parameters Δr and β_3. Next, the algorithm checks if the following constraint is satisfied

$$[d_l^{k+1}, d_r^{k+1}] \bigcap \left(\bigcup_{i=1}^{k} [d_l^i, d_r^i] \right) \neq \emptyset, \tag{20}$$

without taking into account the error in the ANN MP-LROM model prediction. This is achieved by comparing the error model prediction $\widehat{\log \varepsilon}^{HF}_{d_l^k,\mu_{p_{k+1}},K_{POD}}$ and threshold $\log \bar{\varepsilon}_{k+1}$ (see instruction 27 and bottom of Fig. 3(a) for $k = 0$). If the predicted error is smaller than the current threshold, assuming a monotonically increasing error with larger distances $d(\mu, \mu_{p_{k+1}})$, the reduced-order model solutions should satisfy the accuracy threshold for all $\mu \in [\mu_{p_{k+1}}, d_l^k]$. In consequence Eq. (20) will be satisfied for the current $\mu_{p_{k+1}}$, if we set $r_{k+1} = \mu_{p_{k+1}} - d_l^k$ (see instruction 30). In the case the error estimate is larger than the present threshold, the centered parameter $\mu_{p_{k+1}}$ is updated to the middle point between old $\mu_{p_{k+1}}$ and d_l^k (see also the bottom of Fig. 3(a)). For the situation where the monotonic property of the error does not hold in practice, a simply safety net is used at instruction 12.

The instructions between lines 5 and 21 generate the μ_{p_k}-feasible interval, for the case when the current centered parameter $\mu_{p_k} \neq d_l^{k-1}$ (see top part of Fig. 3(b) for $k = 1$). Here by *int* we refer to the integer part of a real number. We used the Matlab command floor for the implementation. For situation when $\mu_{p_k} = d_l^{k-1}$ (see bottom of Fig. 3(b) for $k = 2$), the threshold has to be increased (by setting $\bar{\varepsilon}_k = \beta_1 \bar{\varepsilon}_k$ at line 23), since the reduced-order model solutions cannot satisfy the desired precision according to the predicted errors. In consequence, β_1 has to be selected larger than 1. The need for relaxing the threshold suggests that the greedy search is currently operating into a parametric region where only a slight change in the parameter μ away from μ_{p_k} leads to predicted ROM errors larger than the current threshold. Relaxing the threshold and decreasing the radius size (select $\beta_2 < 1$ in line 23 of Algorithm 2) can be used as a strategy to identify a feasible region for the current centered parameter μ_{p_k}. Similarly, relaxing the threshold and expanding the search ($\beta_2 > 1$) could also represent a viable strategy. However, expanding the search in a parametric regime with large changes in the model dynamics, even if the threshold was relaxed, may lead to useless evaluations of the expressions in lines 7 and 18 of the Algorithm 2. Thus β_2 should be selected smaller than 1. Once the feasible region is obtained, the radius r_k is reset to the initial value r_0 (see line 25 of the Algorithm 2). By selecting $\beta_3 > 1$, the computational complexity of Algorithm 2 is decreased since the first proposal of the new centered parameter $\mu_{p_{k+1}}$ will always be smaller than the left limit d_l^k of the current feasible interval. The entire algorithm stops when $\mu_{p_{k+1}} \leq A$.

For our experiments we set $A = 0.01$, $B = 1$, $\bar{\varepsilon}_0 = 10^{-2}$, $\Delta r = 5 \times 10^{-3}$, $r_0 = 0.5$, $K_{POD} = 9$, $\beta_1 = 1.2$, $\beta_2 = 0.9$ and $\beta_3 = 1.4$. We initiate the algorithm by setting $\mu_{p_0} = 0.87$, and the first feasible interval [0.7700, 1] is obtained. Next the algorithm selects $\mu_1 = 0.73$ with the associated range of [0.6700, 0.8250] using the same initial threshold level. As we cover the parametric domain from right to left; i.e., selecting smaller and smaller parameters μ_{p_k}, the algorithm enlarges the current threshold $\bar{\varepsilon}_k$, otherwise the error model predictions would not satisfy the initial precision. We continue this process until we get the threshold 6.25 with $\mu_{32} = 0.021$ and the corresponding feasible interval [0.01, 0.039]. The generated decomposition is depicted in Fig. 4 where the associated threshold varies with the parameter change.

Algorithm 2 Generation of 1D-parametric domain decomposition for reduced-order models usage. Extension to multi-dimensional parametric space is subject to future research.

1: Select μ_{p_0} as the right edge of the parameter interval, i.e. $\mu_{p_0} = B$.
2: Set error threshold $\hat{\varepsilon}_0$, step size Δr for selection of sampling parameters μ, the maximum search radius r_0, dimension of POD basis K_{POD} and β_1, β_2 and β_3.
3: Set $k = 0$.
4: WHILE $\mu_{p_k} \geq A$ Do
5: FOR $i = 1$ to $int(\frac{r_k}{\Delta r}) + 1$
6: Set $\mu = \mu_{p_k} + i\Delta r$
7: IF ($\phi(\mu, \mu_{p_k}, K_{POD}) > \log \bar{\varepsilon}_k$ OR $\mu > B$) THEN
8: Set $d_r^k = \mu_{p_k} + (i-1)\Delta r$. EXIT.
9: END IF
10: END FOR
11: IF $k > 0$ THEN
12: IF $d_r^k < d_l^{k-1}$ THEN
13: $\mu_{p_k} = \frac{\mu_{p_k} + d_l^{k-1}}{2}$. GOTO 5.
14: END IF
15: END IF
16: FOR $j = 1$ to $int(\frac{r_k}{\Delta r}) + 1$
17: Set $\mu = \mu_{p_k} - j\Delta r$
18: IF ($\phi(\mu, \mu_{p_k}, K_{POD}) > \log \bar{\varepsilon}_k$ OR $\mu < A$) THEN
19: Set $d_l^k = \mu_{p_k} - (j-1)\Delta r$. EXIT.
20: END IF
21: END FOR
22: IF ($i = 1$) .OR. ($j = 1$) THEN
23: Set $\bar{\varepsilon}_k = \beta_1 \cdot \bar{\varepsilon}_k$; $r_k = \beta_2 \cdot r_k$; GOTO 5.
24: ELSE
25: $\mu_{p_{k+1}} = \mu_{p_k} - \beta_3(j-1)\Delta r$; $\bar{\varepsilon}_{k+1} = \bar{\varepsilon}_k$; $r_{k+1} = r_0$.
26: END IF
27: WHILE $\phi(d_l^k, \mu_{p_{k+1}}, K_{POD}) > \log \bar{\varepsilon}_{k+1}$ DO
28: $\mu_{p_{k+1}} = \frac{\mu_{p_{k+1}} + d_l^k}{2}$.
29: END WHILE
30: Set $r_{k+1} = \mu_{p_{k+1}} - d_l^k$.
31: $k = k + 1$.
32: END WHILE

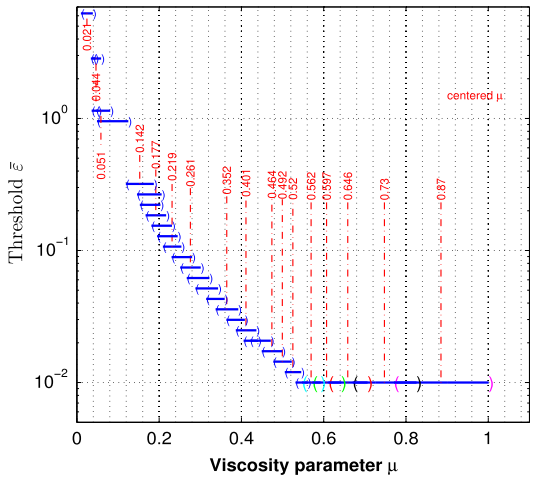

Fig. 4. The diffusion parametric domain decomposition defining the local feasible intervals and their corresponding errors. Associated with one feasible interval there is a centered parameter μ_p high-fidelity trajectory that guides the construction of a reduced basis and operators such that the subsequent reduced-order model solutions along this interval are accurate to within the threshold depicted by the Y-axis labels.

4.3. Combining available information for accurate local ROMs at arbitrary parametric configurations

We now use the available database of local bases and reduced-order models resulted from the parameter decomposition to construct a new POD basis for a different parameter configuration μ^* leading to more accurate reduced-order model solution. The numerical experiments described here focus on the construction of a POD basis for $\mu^* = 0.35$ by combining the basis data or high fidelity results data available from existing simulations with $\mu_{p_1} = 0.3$ and $\mu_{p_2} = 0.4$.

The performances of the discussed methods (bases concatenation, Lagrange interpolation of bases in the matrix space and in the tangent space of the Grassmann manifold, Lagrange interpolation of high-fidelity solutions) are shown in the case of three main experiments: variation in the final time t_f, in the non-linear advection coefficient ν and POD basis dimension. The bases concatenation method followed by orthogonalization is referred as Gram–Schmidt whereas the Lagrange interpolation of bases and high-fidelity solutions are simply described as "Lagrange bases" and "Lagrange sol" in the legends of Figs. 5 and 6. All the methods employ reduced bases having the same dimension. Only even basis dimensions are utilized and the concatenation method combines half of the modes of each involved bases. This strategy was selected based on the spectra of the snapshots matrices associated with $\mu_{p_1} = 0.3$ and $\mu_{p_2} = 0.4$. More precisely, we selected the first $\frac{K_{POD}}{2}$ singular vectors from each of the bases since for all our experiments $\lambda^{\mu_{p_1}}_{\frac{K_{POD}}{2}} > \lambda^{\mu_{p_2}}_{\frac{K_{POD}}{2}+1}$ and $\lambda^{\mu_{p_2}}_{\frac{K_{POD}}{2}} > \lambda^{\mu_{p_1}}_{\frac{K_{POD}}{2}+1}$, where $\lambda^{\mu_{p_1}}_{\frac{K_{POD}}{2}+1}$ denotes the singular value corresponding to the first singular vector associated with trajectory μ_{p_1} not taken into account in the POD expansion. Of course this choice is not optimal. The optimal solution can be obtained by solving a combinatorial optimization problem, where the searched space has the size of $2K_{POD}$ chose K_{POD}.

The first two experiments scale the time and space and modify the linear and nonlinear characteristics of the model. For example, in the case of a tiny small final time and advection coefficient, the diffusion linear part represents the main dynamical engine of the model thus it behaves linearly. The results are compared against reduced-order models constructed using $U_{\mu_{p_1}}$ and $U_{\mu_{p_2}}$, respectively.

Fig. 5 illustrates the Frobenius norm error between the high fidelity and reduced-order model solutions for the final time $t_f = 0.01$. Panel (a) presents the accuracy results as a function of the advection coefficient ν. Interpolating the high-fidelity solutions leads to the most accurate reduced-order model. For large advection coefficients all of the methods suffer accuracy losses. Among the potential explanations we include the constant dimension of the POD basis and the linear dependence on the viscosity parameter assumed by all of the methods in various forms. Fig. 5(b)) shows that the basis dimension must be increased as the advection coefficient decreases to maintain constant error.

Since the Grassmann manifold approach is a generalization of the subspace angle interpolation method we decide to show only the results corresponding to the former method. While Lagrangian interpolation of the bases is performed in both matrix space and tangent space of the Grassmann manifold (shown in cyan and green), the later approach performs better in this scenario. The concatenation of bases using Gram–Schmidt algorithm was successful only for larger advection coefficients (red curve in Fig. 5(a)), for a POD dimension set to 14.

Increasing the dimension of the basis enhances the so called Gram–Schmidt reduced-order model solution accuracy for $\nu = 1$ (see Fig. 5(b)). For this case Lagrange interpolation in the matrix space shows better performances in comparison with the output of the Grassmann manifold approach.

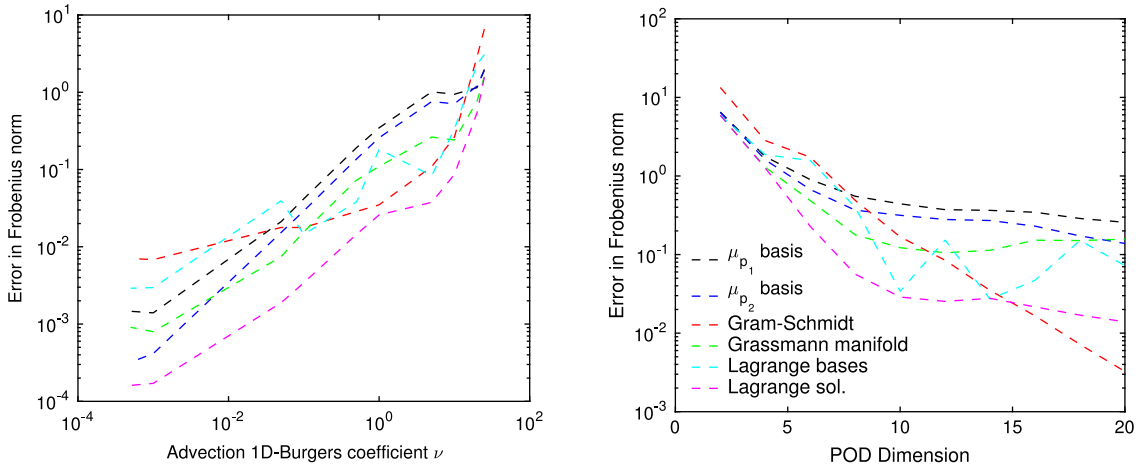

(a) The nonlinearity model variations. (b) Dimension of POD basis variation.

Fig. 5. Strategies comparison for generation of accurate ROMs for a new viscosity parameter $\mu^* = 0.35$ and $t_f = 0.01$. In panel (a) K_{POD} is set to 14, whereas in panel (b) ν is set to 1. (For interpretation of the references to color in this figure legend, the reader is referred to the web version of this article.)

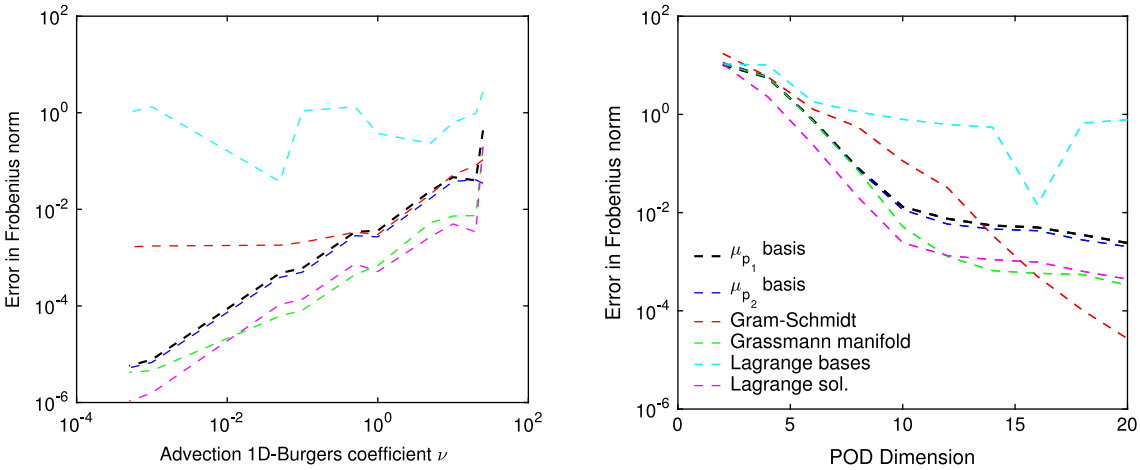

(a) The nonlinearity model variations. (b) Dimension of POD basis variation.

Fig. 6. Strategies comparison for generation of accurate ROMs for a new viscosity parameter $\mu^* = 0.35$ and $t_f = 1$. In panel (a) K_{POD} is set to 14, whereas in panel (b) ν is set to 1.

Next we increase the nonlinearity characteristics of the model by setting the final time to $t_f = 1$ and Fig. 6 illustrates the Frobenius norm errors as a function of the advection coefficient ν and POD dimension. The errors produced by the reduced-order model derived via Grassmann manifold method are similar with the ones obtained by the surrogate model relying on a POD basis computed via the Lagrange interpolation of the high-fidelity model solutions.

The Lagrange interpolation of bases in the matrix space is not successful as seen in both panels of Fig. 6. Increasing the POD dimension to 20, the Gram–Schmidt approach enhances the accuracy of the solution (see Fig. 6(b)), for $\nu = 1$.

5. Conclusions

This study develops a new and efficient methodology for constructing reduced-order surrogates for parametric high-fidelity models. We demonstrate the value of MP-LROM error model to generate accurate description of the local reduced-order models errors along the entire parametric domain.

The MP-LROM error prediction and parametric domain sampling are utilized to generate decompositions of the space of parameters into overlapping sub-regions. For each region an associated local reduced-order basis and operators are constructed using snapshots from a single representative high-fidelity trajectory. The procedure guarantees that, that for

all values of the parameters in a region, the high-fidelity model is approximated by the same local reduced-order surrogate within a feasible prescribed accuracy level. Under specific conditions, we derived a theoretical lower limit for the accuracy level of a local parametric reduced-order model associated with a parametric sub-region. The novel methodology was applied to a 1D-Burgers model. A decomposition of the viscosity parameter interval into sub-intervals with associated errors thresholds was performed.

Next we employed the hierarchy of local bases, local reduced-order and high-fidelity models producing the most accurate solutions for an arbitrary parameter configuration. Based on this hierarchy, three already existing methods involving bases interpolation and concatenation and high-fidelity model solutions interpolation were applied to enhance the quality of the associated reduced-order model solutions. Several experiments were performed by scaling the time and space and modifying the nonlinear characteristics of the 1D-Burgers model. In most cases, interpolating the already existing high-fidelity trajectories generated the most accurate reduced-order models for a new viscous parameter revealing that the solution behavior over the parametric region under study can be linearly approximated. Lagrange interpolation of bases in the tangent space of the Grassmann manifold and concatenation of bases for larger reduced subspaces also showed good performances.

This work illustrates the rich potential of machine learning to impact the field of computational science and engineering. The new methodology ensures that a small number of reduced-order models can approximate well the high-fidelity model solutions for all parametric configurations. This greatly decreases overall computational costs since reduced-order models are expensive to construct. In the present work the parametric domain decomposition algorithm is applied to a one-dimensional parameter space.

As a future work, we seek to decrease the computational complexity of the MP-LROM error models. Currently the training data required by the machine learning MP-LROM models relies on many high-fidelity simulations. By employing error bounds, residual norms [22] and a-posteriori error estimation results [52,38], this dependency can be much decreased. In addition, we plan to construct machine learning MP-LROM models to estimate the errors in quantities of interest computed with reduced-order models. The predictions of such error models can then be used to speed up the current trust-region reduced-order framework [53,54] by eliminating the need of high-fidelity simulations for the quality evaluation of the updated controls.

Moreover, we are investigating the extension of the methodology to multi-dimensional parametric domains based on multivariate sampling. In order to address the curse of dimensionality, we plan to combine our methodology with the active subspace method [55] to efficiently design decompositions of high-dimensional parametric problems.

Acknowledgments

This work was supported in part by awards from National Science Foundation CCF-1613905, AFOSR DDDAS 15RT1037, AFOSR Computational Mathematics (FA9550-17-1-0205), and by the Computational Science Laboratory at Virginia Tech. Răzvan Ştefănescu thanks Dr. Dan Ştefănescu for his valuable suggestions on the machine learning topic.

References

[1] B. Noack, M. Schlegel, M. Morzynski, G. Tadmor, Galerkin Method for Nonlinear Dynamics, in: B. Noack, M. Morzynski, G. Tadmor (Eds.), Reduced-Order Modelling for Flow Control, Vol. 528, Springer, 2011, pp. 111–149.
[2] M. Hinze, S. Volkwein, Proper orthogonal decomposition surrogate models for nonlinear dynamical systems: Error estimates and suboptimal control, in: Dimension Reduction of Large-Scale Systems, Springer, 2005, pp. 261–306.
[3] C. Prud'homme, D.V. Rovas, K. Veroy, L. Machiels, Y. Maday, A.T. Patera, G. Turinici, Reliable real-time solution of parametrized partial differential equations: Reduced-basis output bound methods, J. Fluids Eng. 124 (1) (2002) 70–80.
[4] B.R. Noack, P. Papas, P.A. Monkewitz, The need for a pressure-term representation in empirical Galerkin models of incompressible shear flows, J. Fluid Mech. 523 (2005) 339–365.
[5] R. Prabhu, S.S. Collis, Y. Chang, The influence of control on proper orthogonal decomposition of wall-bounded turbulent flows, Phys. Fluids 13 (2) (2001) 520–537.
[6] B.R. Noack, K. Afanasiev, M. Morzyński, G. Tadmor, F. Thiele, A hierarchy of low-dimensional models for the transient and post-transient cylinder wake, J. Fluid Mech. 497 (2003) 335–363.
[7] J. Burkardt, M. Gunzburger, H. Lee, POD and CVT-based reduced-order modeling of Navier–Stokes flows, Comput. Methods Appl. Mech. Engrg. 196 (1–3) (2006) 337–355.
[8] J.L. Eftang, B. Stamm, Parameter multi-domain 'hp' empirical interpolation, Internat. J. Numer. Methods Engrg. 90 (4) (2012) 412–428.
[9] M. Rapún, J. Vega, Reduced order models based on local POD plus Galerkin projection, J. Comput. Phys. 229 (8) (2010) 3046–3063.
[10] M. Dihlmann, M. Drohmann, B. Haasdonk, Model reduction of parametrized evolution problems using the reduced basis method with adaptive time-partitioning, in: Proc. of ADMOS 2011, 2011.
[11] B. Peherstorfer, D. Butnaru, K. Willcox, H.-J. Bungartz, Localized discrete empirical interpolation method, SIAM J. Sci. Comput. 36 (1) (2014) A168–A192.
[12] S. Kaulmann, B. Haasdonk, Online greedy reduced basis construction using dictionaries, in: I. Troch, F. Breitenecker (Eds.), Proceedings of 7th Vienna International Conference on Mathematical Modelling, 2012, pp. 112–117.
[13] Y. Maday, B. Stamm, Locally adaptive greedy approximations for anisotropic parameter reduced basis spaces, SIAM J. Sci. Comput. 35 (6) (2013) A2417–A2441.
[14] M.A. Grepl, A.T. Patera, A posteriori error bounds for reduced-basis approximations of parametrized parabolic partial differential equations, ESAIM Math. Model. Numer. Anal. 39 (1) (2005) 157–181.
[15] B. Tracey, K. Duraisamy, J. Alonso, Application of supervised learning to quantify uncertainties in turbulence and combustion modeling, in: 51st AIAA Aerospace Sciences Meeting including the New Horizons Forum and Aerospace Exposition, 2013, p. 259.

[16] J. Ling, J. Templeton, Evaluation of machine learning algorithms for prediction of regions of high reynolds averaged navier stokes uncertainty, Phys. Fluids 27 (8) (2015) 085103.
[17] B.D. Tracey, Machine learning for model uncertainties in turbulence models and monte carlo integral approximation, Ph.D. thesis, Stanford University, 2015.
[18] N.M. Alexandrov, R.M. Lewis, C.R. Gumbert, L.L. Green, P.A. Newman, Approximation and model management in aerodynamic optimization with variable-fidelity models, J. Aircr. 38 (6) (2001) 1093–1101.
[19] M. Eldred, A. Giunta, S. Collis, N. Alexandrov, R. Lewis, Second-order corrections for surrogate-based optimization with model hierarchies, in: Proceedings of the 10th AIAA/ISSMO Multidisciplinary Analysis and Optimization Conference, Albany, NY, Aug, 2004, pp. 2013–2014.
[20] S.E. Gano, J.E. Renaud, B. Sanders, Hybrid variable fidelity optimization by using a kriging-based scaling function, AIAA J. 43 (11) (2005) 2422–2433.
[21] D. Huang, T. Allen, W. Notz, R. Miller, Sequential kriging optimization using multiple-fidelity evaluations, Struct. Multidiscip. Optim. 32 (5) (2006) 369–382.
[22] M. Drohmann, K. Carlberg, The ROMES method for statistical modeling of reduced-order-model error, SIAM/ASA J. Uncertain. Quantif. 3 (1) (2015) 116–145.
[23] A. Moosavi, R. Ştefănescu, A. Sandu, Multivariate predictions of local reduced-order-model errors and dimensions, Int. J. Numer. Methods Eng. n/a–n/a, http://dx.doi.org:101002/nme.5624.
[24] T. Lieu, M. Lesoinne, Parameter adaptation of reduced order models for three-dimensional flutter analysis, AIAA Paper 888 (2004) 2004.
[25] D. Amsallem, C. Farhat, An interpolation method for adapting reduced-order models and application to aeroelasticity, AIAA J. 46 (7) (2008) 1803–1813.
[26] G. Weickum, M. Eldred, K. Maute, Multi-point extended reduced order modeling for design optimization and uncertainty analysis, in: Proceedings of the 47th AIAA/ASME/ASCE/AHS/ASC Structures, Structural Dynamics, and Materials Conference (2nd AIAA Multidisciplinary Design Optimization Specialist Conference), Newport, RI, 2006, pp. 2006–2145.
[27] C.W. Rowley, T. Colonius, R.M. Murray, Model reduction for compressible flows using POD and Galerkin projection, Physica D 189 (1) (2004) 115–129.
[28] K. Kunisch, S. Volkwein, Galerkin proper orthogonal decomposition methods for a general equation in fluid dynamics, SIAM J. Numer. Anal. 40 (2) (2002) 492–515.
[29] C. Rowley, Model reduction for fluids, using balanced proper orthogonal decomposition, Int. J. Bifur. Chaos (IJBC) 15 (3) (2005) 997–1013.
[30] K. Willcox, J. Peraire, Balanced model reduction via the proper orthogonal decomposition, AIAA J. (2002) 2323–2330.
[31] G. Rozza, D.B.P. Huynh, A.T. Patera, Reduced basis approximation and a posteriori error estimation for affinely parametrized elliptic coercive partial differential equations, Arch. Comput. Methods Eng. 15 (3) (2008) 229–275.
[32] A. Quarteroni, G. Rozza, A. Manzoni, Certified reduced basis approximation for parametrized partial differential equations and applications, J. Math. Ind. 1 (1) (2011) 1–49.
[33] J. Taylor, M. Glauser, Towards practical flow sensing and control via POD and LSE based low-dimensional tools, J. Fluids Eng. 126 (3) (2004) 337–345.
[34] R. Schmit, M. Glauser, Improvements in low dimensional tools for flow-structure interaction problems: using global POD, in: APS Division of Fluid Dynamics Meeting Abstracts, Vol. 1, 2003.
[35] L. Daniel, O.C. Siong, L.S. Chay, K.H. Lee, J. White, A multiparameter moment-matching model-reduction approach for generating geometrically parameterized interconnect performance models, IEEE Trans. Comput.-Aided Des. Integr. Circuits Syst. 23 (5) (2004) 678–693.
[36] D. Weile, E. Michielssen, E. Grimme, K. Gallivan, A method for generating rational interpolant reduced order models of two-parameter linear systems, Appl. Math. Lett. 12 (5) (1999) 93–102.
[37] B. Haasdonk, M. Ohlberger, Reduced Basis Method for Finite Volume Approximations of Parametrized Linear Evolution Equations, ESAIM Math. Model. Numer. Anal. 42 (2) (2008) 277–302.
[38] N.-C. Nguyen, G. Rozza, A.T. Patera, Reduced basis approximation and a posteriori error estimation for the time-dependent viscous Burgers' equation, Calcolo 46 (3) (2009) 157–185.
[39] D.E. Rumelhart, G.E. Hinton, R.J. Williams, Learning internal representations by error propagation, Tech. Rep., DTIC Document, 1985.
[40] K.-I. Funahashi, On the approximate realization of continuous mappings by neural networks, Neural Netw. 2 (3) (1989) 183–192.
[41] S. Haykin, Neural Networks and Learning Machines, in: Neural Networks and Learning Machines, vol. 10, Prentice Hall, 2009. URL https://books.google.com/books?id=K7P36lKzI_QC.
[42] T. Lassila, A. Manzoni, A. Quarteroni, G. Rozza, Generalized reduced basis methods and n-width estimates for the approximation of the solution manifold of parametric PDEs, in: Analysis and Numerics of Partial Differential Equations, Springer, 2013, pp. 307–329.
[43] P.-A. Absil, R. Mahony, R. Sepulchre, Riemannian geometry of Grassmann manifolds with a view on algorithmic computation, Acta Appl. Math. 80 (2) (2004) 199–220.
[44] A. Edelman, T.A. Arias, S.T. Smith, The geometry of algorithms with orthogonality constraints, SIAM J. Matrix Anal. Appl. 20 (2) (1998) 303–353.
[45] E. Begelfor, M. Werman, Affine invariance revisited, in: Proceedings of the 2006 IEEE Computer Society Conference of Computer Vision and Pattern Recognition, Vol. 2, 2006, pp. 2087–2094.
[46] T. Lieu, C. Farhat, M. Lesoinne, POD-based aeroelastic analysis of a complete F-16 configuration: ROM adaptation and demonstration, AIAA Paper 2295 (2005) 2005.
[47] S. Volkwein, Proper orthogonal decomposition: applications in optimization and control, CEA-EDFINRIA Numerical Analysis Summer School, 2007.
[48] G.H. Golub, C.F. Van Loan, Matrix Computations, fourth ed., JHU Press, Baltimore, 2013.
[49] T.F. Chan, An improved algorithm for computing the Singular Value Decomposition, ACM Trans. Math. Softw. (TOMS) 8 (1) (1982) 72–83.
[50] J.M. Burgers, A mathematical model illustrating the theory of turbulence, Adv. Appl. Mech. 1 (1948) 171–199.
[51] R. Ştefănescu, A. Sandu, I.M. Navon, Comparison of POD reduced order strategies for the nonlinear 2D shallow water equations, Internat. J. Numer. Methods Fluids 76 (8) (2014) 497–521.
[52] M. Gubisch, I. Neitzel, S. Volkwein, A-posteriori error estimation of discrete POD models for PDE-constrained optimal control, Tech. Rep., Konstanzer Schriften in Mathematik, 2016.
[53] E. Arian, M. Fahl, E.W. Sachs, Trust-region proper orthogonal decomposition for flow control, ICASE, Tech. Rep. 2000-25, 2000.
[54] M. Bergmann, L. Cordier, Optimal control of the cylinder wake in the laminar regime by trust-region methods and POD reduced-order models, J. Comput. Phys. 227 (16) (2008) 7813–7840.
[55] P.G. Constantine, E. Dow, Q. Wang, Active subspace methods in theory and practice: applications to kriging surfaces, SIAM J. Sci. Comput. 36 (4) (2014) A1500–A1524.